PDI-Based Heteroacenes as Acceptors for Fullerene-free Solar Cells: Importance of the Twisted Geometry

Huaqing Chen,[†] Ling Wang,[†] Hua Sun,[§] Qian Liu,[†] Xiao Tan,[†] Shenglong Sang,[†] Bo Wu,[†] Cong Zhang,[†] Fei Chen,[*,†,‡] Xiao-Chun Hang,[*,†] and Zhi-Kuan Chen,[*,†,‡]

[†]*Key Laboratory of Flexible Electronics (KLOFE) & Institute of Advanced Materials (IAM), Nanjing Tech University, 30 South Puzhu Road, Nanjing, 211816 (P. R. China)*

[‡]*Department of Mechanical, Materials and Manufacturing Engineering and Department of Chemical and Environmental Engineering, The University of Nottingham, Ningbo China, 199 Taikang East Road, Ningbo 315100, P. R. China*

[§]*School of Material and Chemistry Engineering, Xuzhou University of Technology, Xuzhou, China*

AUTHOR INFORMATION
Corresponding Author
*E-mail: fei.chen@nottingham.edu.cn (F. C.)
*E-mail: iamxchhang@njtech.edu.cn (X.-C. H.)
*E-mail: zhikuan.chen@nottingham.edu.cn (Z.-K. C.)

Experimental Section

1. Materials

All reagents and chemicals were purchased from commercial sources and used without further purification unless stated otherwise. Toluene were freshly distilled before use by sodium drying. PTB7-Th was purchased from 1-Material (Canada). FPDI-T were synthesized according to literature procedures.[1]

2. Synthesis and Characterization

2.1

2.1 FPDI-T-Br

FPDI-T (7.93 g, 5.00 mmol) was dissolved in $CHCl_3$ (100 mL). Bromine (10 mL) was then added, and the solution was stirred at 30 °C for 48 h. The reaction was quenched with sodium thiosulfate solution and extracted twice with $CHCl_3$. The combined organics were washed with water, dried over Na_2SO_4, and filtered. The residue was purified by flash column chromatography (eluent: n-hexane/dichloromethane = 2:1) to obtain a red solid (3.75 g, 45%) as the product; ^{1}H NMR (400 MHz, $CDCl_3$) δ (ppm): 10.79-10.49 (m, 3H), 9.92 (d, J = 11.6 Hz, 2H), 9.60-9.31 (m, 3H), 9.13(s, 3H), 5.37 (m, 4H), 2.52-2.24 (m, 8H), 2.05-1.86 (m, 8H), 1.09-1.49 (m, 64H), 0.94-0.64 (m, 24H). ^{13}C NMR (100MHz, $CDCl_3$, 300K): δ 164.60, 163.88, 140.98, 140.74, 137.02, 133.33, 132.98, 132.56, 132.04, 131.68, 131.17, 130.10, 129.38, 128.90, 127.85, 127.51, 127.03, 126.67, 126.23, 125.90, 125.48, 125.31, 124.84, 124.39, 123.77, 123.50, 122.38, 121.17, 55.27, 32.47, 32.18, 31.84, 30.24, 29.31, 27.09, 23.06, 22.65, 22.47, 14.20, 14.10, 13.95. MS (MALDI-TOF) m/z: calcd. for $C_{104}H_{119}BrN_4O_8S$: 1665.79; found: 1665.85.

2.2 $P_4$3T

Under N_2 atmosphere, a mixture of 2,5-bis(trimethylstannyl)thiophene (148 mg, 0.36 mmol), FPDI-T-Br (1.20 g, 0.72 mmol), $Pd(PPh_3)_4$ (24 mg, 0.02 mmol), and toluene (120 mL) were heated to 110 °C for 48 h. The reaction mixture was then cooled to room temperature and extracted twice with $CHCl_3$. The organic layer was combined, washed with brine, dried over Na_2SO_4, and filtered. The residue was purified by flash column chromatography (eluent: n-hexane/dichloromethane = 1:1) to obtain a black violet solid (749 mg, 64%) as the product; ^{1}H NMR (400 MHz, $CDCl_3$) δ (ppm): 10.77-10.55 (m, 4H), 9.96 (s, 4H), 9.70-9.26 (m, 8H), 9.17 (s, 4H), 8.98 (s, 2H), 7.71 (s, 2H), 5.38 (s, 8H), 2.53-2.24 (m, 16H), 1.87-2.07 (m, 16H), 1.49-1.06 (m, 128H), 0.96-0.66 (m, 48H). ^{13}C NMR (100 MHz, $CDCl_3$, 323K): Numerous carbon resonances overlap, leading to less signals than the number of carbons. δ 164.80, 163.94, 147.69, 144.30, 140.81, 133.53, 133.19, 132.30, 131.28, 130.22, 129.54, 128.96, 127.64, 127.18, 126.19, 125.64, 125.01, 124.56, 124.07, 123.81, 123.61, 123.21, 122.44, 55.29, 54.70, 32.57, 32.20, 31.83, 30.26, 29.34, 27.10, 26.95, 23.08, 22.66, 22.47, 14.10. MS (MALDI-TOF) m/z: calcd. for $C_{212}H_{240}N_8O_{16}S_3$: 3251.74; found: 3251.75.

2.3 P_4TT2T

Under N_2 atmosphere, a mixture of 2,5-bis(trimethylstannyl)thieno[3,2-b]thiophene (168 mg, 0.36 mmol), FPDI-T-Br (1.20 g, 0.72 mmol),

$Pd(PPh_3)_4$ (24 mg, 0.02 mmol), and toluene (120 mL) were heated to 110 °C for 48 h. The reaction mixture was then cooled to room temperature and extracted twice with $CHCl_3$. The organic layer was combined, washed with brine, dried over Na_2SO_4, and filtered. The residue was purified by flash column chromatography (eluent: n-hexane/dichloromethane = 1:1) to obtain a black violet solid (810 mg, 68%) as the product; ^{1}H NMR (400 MHz, $CDCl_3$) δ (ppm): 10.65 (d, J = 10.3 Hz, 4H), 9.95 (s, 4H), 9.52-9.29 (m, 8H), 9.15 (s, 4H), 8.91 (s, 2H), 7.91 (d, J = 11.7 Hz, 2H), 5.37 (s, 8H), 2.57-2.28 (m, 16H), 2.06-1.87 (m, 16H), 1.47-1.06 (m, 128H), 0.95-0.65 (m, 48H). ^{13}C NMR (100 MHz, $CDCl_3$, 323K): Numerous carbon resonances overlap, leading to less signals than the number of carbons. δ 164.81, 163.86, 149.18, 147.61, 141.83, 140.97, 140.74, 140.17, 138.94, 134.33, 133.41, 133.05, 132.22, 131.58, 131.24, 129.71, 128.90, 127.54, 127.10, 125.61, 125.02, 124.43, 123.78, 123.52, 123.15, 122.39, 119.90, 119.06, 118.86, 116.95, 55.26, 32.78, 32.53, 32.25, 31.86, 31.52, 30.20, 29.72, 29.35, 27.10, 23.10, 22.68, 22.49, 14.13. MS (MALDI-TOF) m/z: calcd. for $C_{214}H_{240}N_8O_{16}S_4$: 3307.72; found: 3307.64.

2.4 $FP_4$3T

Under N_2 atmosphere, $P_4$3T (650 mg, 0.2 mmol) in 50 mL toluene, a solution of $FeCl_3$ (1.62 g, 10 mmol) in 2 mL CH_3NO_2 was added, and then the reactant solution was heated to reflux and kept stirring for 3 h. The

mixture was cooled to room temperature and extracted by $CHCl_3$, and the organic phase was separated, washed by water and brine, dried over anhydrous Na_2SO_4 and concentrated. The crude product was purified by flash chromatography on silica gel (eluent: dichloromethane/hexane = 1:1) to afford $FP_4$3T (403 mg, 62%) as a red solid; ^{1}H NMR (600 MHz, $C_2D_2Cl_4$, 373K) δ (ppm): 11.66 (s, 1H), 11.52-11.22 (m, 2H), 11.15-10.96 (m, 2H), 10.76 (d, J = 53.4 Hz, 2H), 10.58-10.41 (m, 1H), 10.32-10.07 (m, 2H), 9.84-9.45 (m, 6H), 9.46-9.19 (m, 4H), 5.80-5.30 (m, 8H), 2.76-2.49 (m, 20H), 2.32-2.09 (m, 24H), 1.55-1.32 (m, 103H), 1.00 (s, 60H). ^{13}C NMR (100 MHz, $CDCl_3$, 323K): Numerous carbon resonances overlap, leading to less signals than the number of carbons. δ 165.03, 164.32, 163.77, 141.54, 140.14, 133.69, 132.54, 131.92, 129.41, 127.53, 126.32, 125.86, 124.71, 123.94, 123.01, 55.69, 55.31, 32.58, 31.90, 30.34, 29.70, 29.39, 27.20, 23.18, 22.70, 14.55, 14.14. MS (MALDI-TOF, m/z): calcd. for $C_{212}H_{236}N_8O_{16}S_3$, For $[M+H]^+$: 3248.71; found: 3249.03.

2.5 FP_4TT2T

Under N_2 atmosphere, P_4TT2T (650 mg, 0.2 mmol) in 50 mL toluene, a solution of $FeCl_3$ (1.62 g, 10 mmol) in 2 mL CH_3NO_2 was added, and then the reactant solution was heated to reflux and kept stirring for 3 h. The mixture was cooled to room temperature and extracted by $CHCl_3$, and the organic phase was separated, washed by water and brine, dried over

anhydrous Na_2SO_4 and concentrated. The crude product was purified by flash chromatography on silica gel (eluent: dichloromethane/hexane = 1:1) to afford FP_4TT2T (396 mg, 60%) as a red solid; ^1H NMR (600 MHz, $C_2D_2Cl_4$, 373K) δ (ppm): 11.59-10.48 (m, 8H), 10.18 (s, 2H), 9.51 (d, J = 154.0 Hz, 10H), 6.00-4.98 (m, 8H), 2.75-2.39 (m, 24H), 2.29-2.09 (m, 16H), 1.63-1.38 (m, 108H), 1.14-0.89 (m, 60H). ^{13}C NMR (100 MHz, $CDCl_3$, 323K): Numerous carbon resonances overlap, leading to less signals than the number of carbons. δ 164.87, 164.21, 133.73, 133.29, 132.53, 131.84, 131.53, 130.86, 130.28, 130.08, 129.20, 127.45, 126.77, 126.15, 125.69, 125.34, 124.46, 123.91, 123.47, 122.98, 122.07, 121.86, 121.01, 120.75, 120.72, 119.83, 55.80, 55.38, 32.39, 31.94, 29.71, 29.44, 27.18, 22.76, 14.21.MS (MALDI-TOF) m/z: calcd. for $C_{214}H_{236}N_8O_{16}S_4$: 3303.68; found: 3303.25.

2.6 Materials Characterization

^1H and ^{13}C NMR spectra were collected with a Bruker 400 MHz, 600 MHz, and 101 MHz spectrometer. Matrix-assisted laser desorption-ionization time-of-flight mass spectrometry (MALDI-TOF MS) analysis was performed on a Bruker Autoflex II. Thermogravimetric analysis (TGA) was performed on a TA Discovery TGA analyzer under nitrogen with a heating rate of 10 °C min^{-1}. Differential scanning calorimetry (DSC) was performed on a TA Discovery DSC under nitrogen with a heating rate of

10 °C min^{-1}. All of the simulations were performed by density functional theory (DFT) using the B3LYP hybrid functional with basis set 6-31G(d).[2] Electrochemical measurements were performed under nitrogen in deoxygenated 0.1 M solutions of tetra-*n*-butylammonium hexafluorophosphate in dry dichloromethane using a CHI660E electrochemical workstation, a glassy carbon working electrode, a platinum wire auxiliary electrode, and a Ag/AgCl reference electrode. Cyclic voltammograms were recorded at a scan rate of 100 mV s^{-1}. Solution and thin-film UV-visible absorption spectra were recorded on a Shimadzu UV-1750 UV-vis spectrophotometer.

3. Devices Fabrication and Characterization

3.1 OSC Devices Fabrication

The solar cells were fabricated with a structure of ITO/PEDOT:PSS/PTB7-Th:acceptor/PDIN/Al (ITO, indium tin oxide; PEDOT, poly(3,4-ethylenedioxythiopene); PSS, polystyrene sulfonate; PDIN, 2,9-Bis(3-(dimethylamino)propyl)anthra[2,1,9-def:6,5,10-def] diisoquinoline-1,3,8,10 (2H,9H)-tetraone). The patterned ITO glass was pre-cleaned in an ultrasonic bath of acetone and isopropyl alcohol, then treated in an ultraviolet-ozone chamber for 20 min. A thin layer (30 nm) of PEDOT:PSS (Baytron P, now Clevios VP AI 4083, from H. C. Starck, Leverkusen, Germany) was spin-coated onto the ITO glass and baked at 150 °C for 15

min. A solution (total of 20 mg mL^{-1} dissolved in chlorobenzene) of PTB7-Th:acceptor blend was subsequently spin-coated (2000 rpm) on the PEDOT:PSS layer to form a photosensitive layer (~100 nm thick). The thickness of the photosensitive layer was measured using an Ambios Technology (Santa Cruz, CA) XP-2 profilometer. The methanolic solution (0.2% acetic acid) of PDIN at a concentration of 1.5 mg mL^{-1} was deposited on the active layer at 3000 rpm for 30 s, producing a PDIN layer of ~13 nm. The aluminum layer (~100 nm) was deposited onto the surface of the PDIN layer subsequently through a shadow mask by thermal evaporation under vacuum (~10^{-5}Pa) to form the cathode.

The *J-V* curves of the prepared devices were measured with a computer-controlled Keithley (Zolix ss150 Solar Simulator) 236 source measure unit. A xenon lamp coupled with AM1.5 solar spectrum filters was used as the light source, the optical power at the sample was 100 mW cm^{-2}. The light intensity of the solar simulator was calibrated using a standard silicon solar cell. The external quantum efficiency (EQE) spectra of the devices were measured using a solar cell quantum efficiency measurement system (Zolix Solar cell scan 100), consisting of model SR830 DSP lock-in amplifier coupled with a WDG3 monochromator and a 500 W xenon lamp.

3.2. Space Charge-Limited Current Method Measurement

The transport properties of the devices were evaluated using the space

charge-limited current model with a HP4155A semiconductor parameter analyzer (Yokogawa Hewlett-Packard, Tokyo, Japan). The carrier mobility was extracted by fitting the *J*-*V* curves in the near-quadratic region according to the modified Mott-Gurney equation[3]:

$$J = \frac{9}{8}\varepsilon\varepsilon_0\mu\frac{V^2}{L^3}\left(0.89\beta\frac{\sqrt{V}}{\sqrt{L}}\right) \quad (1)$$

where J is the current density, ε_0 is the permittivity of free space, ε is the relative permittivity, μ is the zero-field mobility, V is the applied voltage, L is the thickness of the active layer, and β is the field-activation factor.

3. Figures and Tables

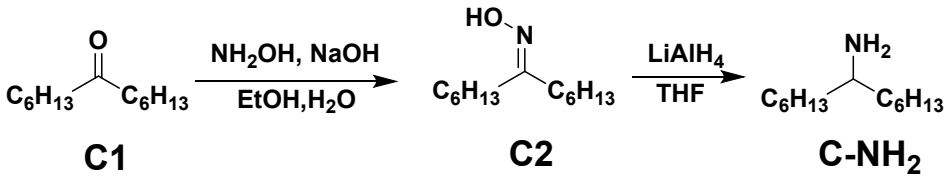

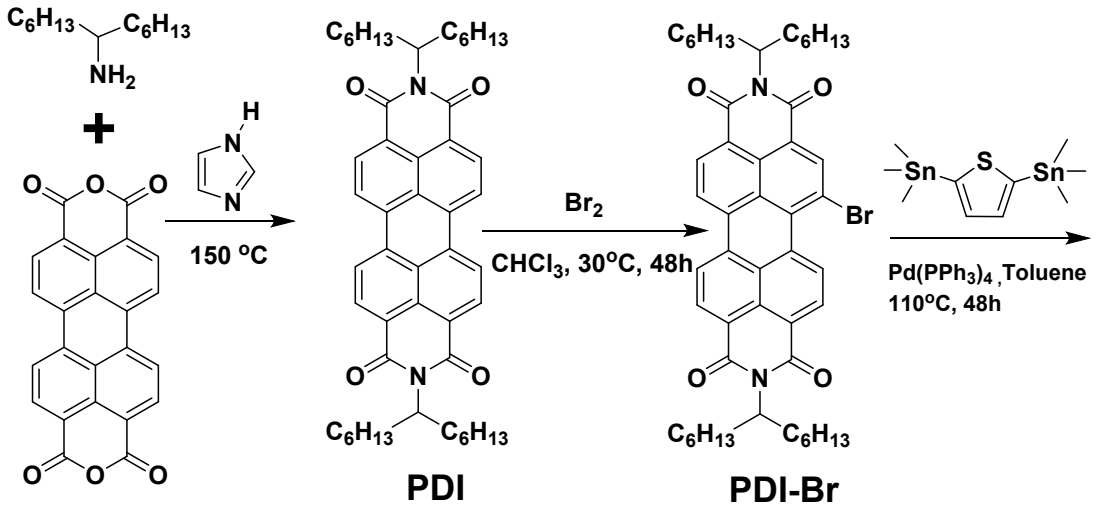

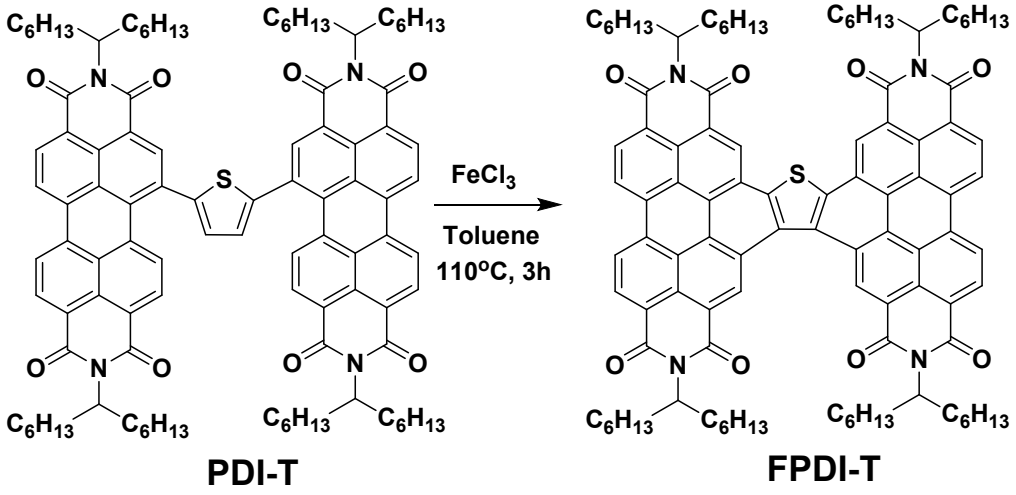

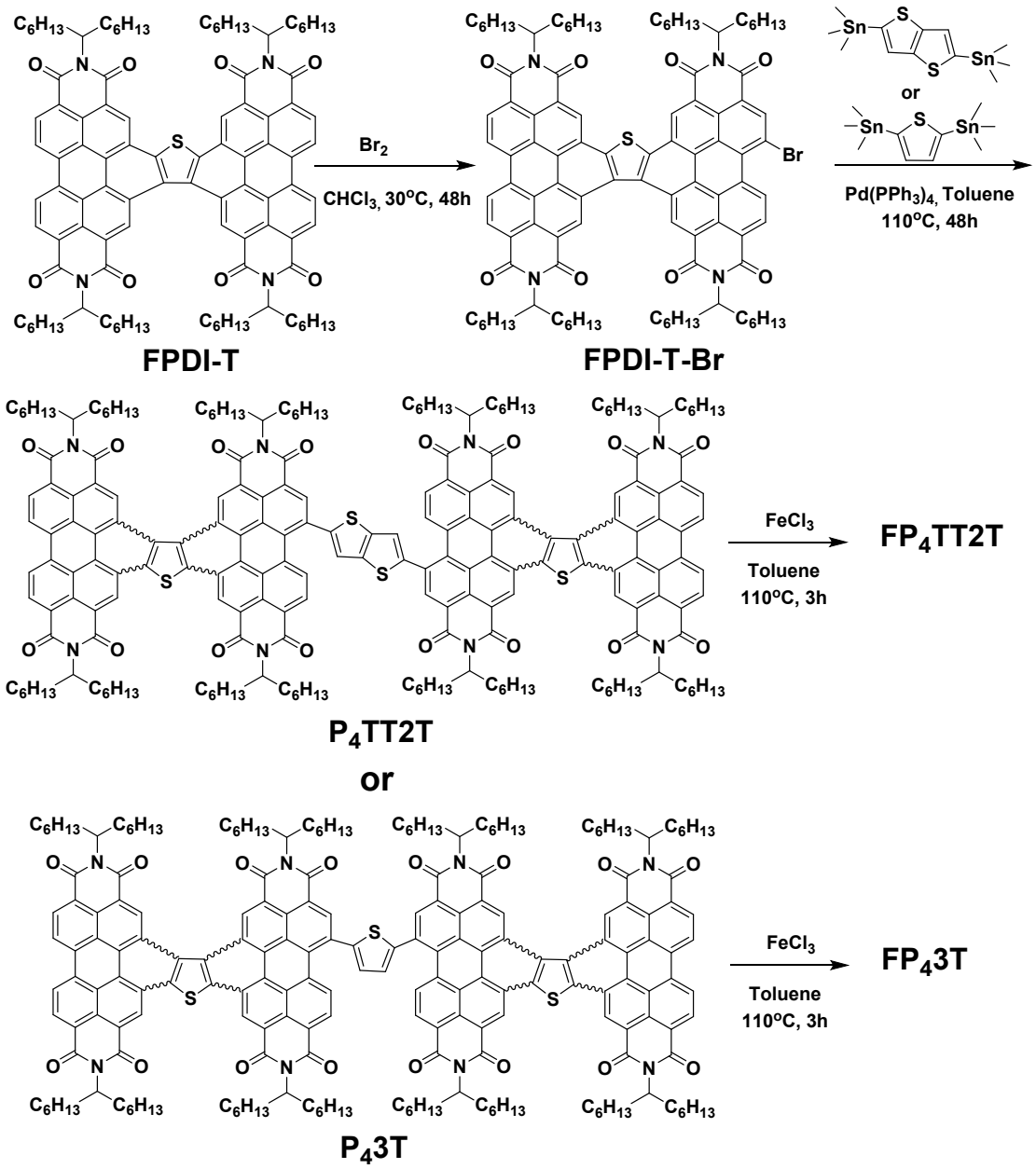

Scheme S1. Synthesis route of $FP_4$3T and FP_4TT2T.

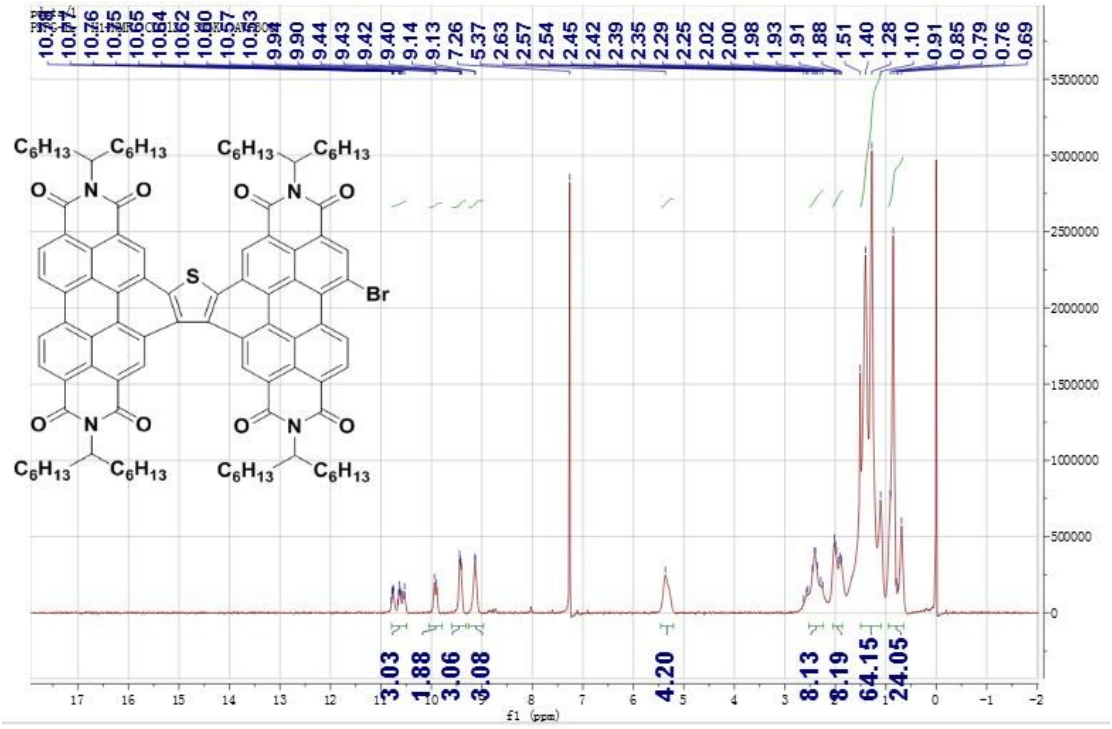

Figure S1. ^{1}H NMR spectrum of FPDI-T-Br.

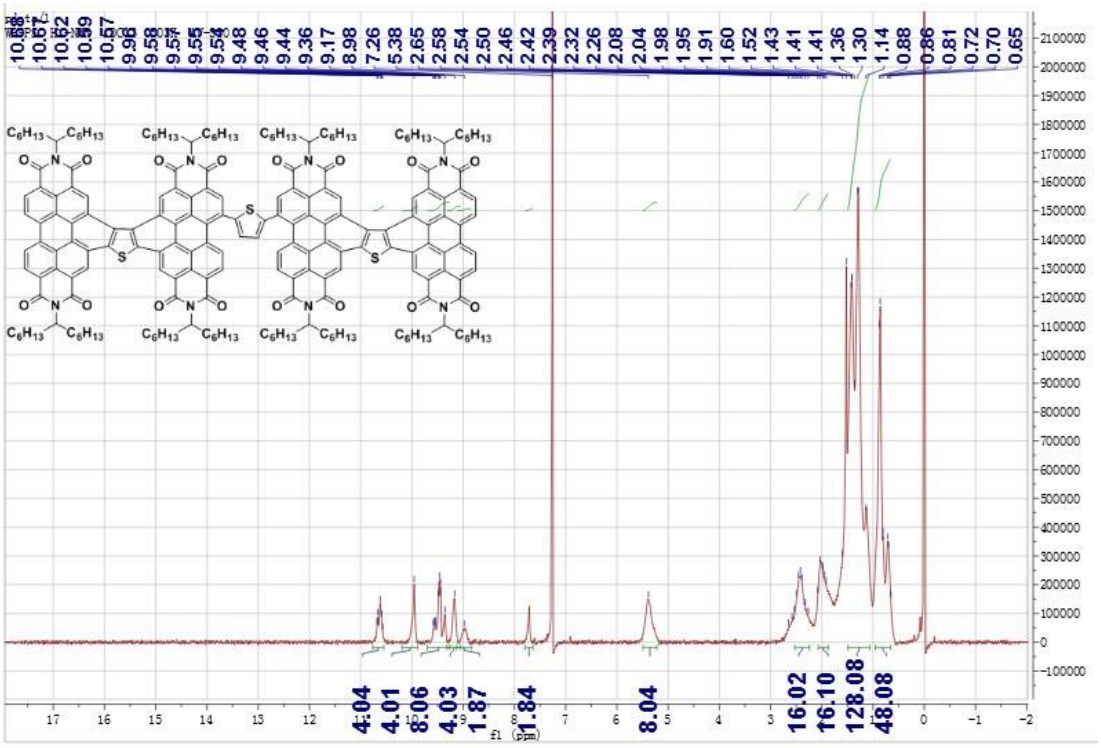

Figure S2. ^{1}H NMR spectrum of $P_4$3T.

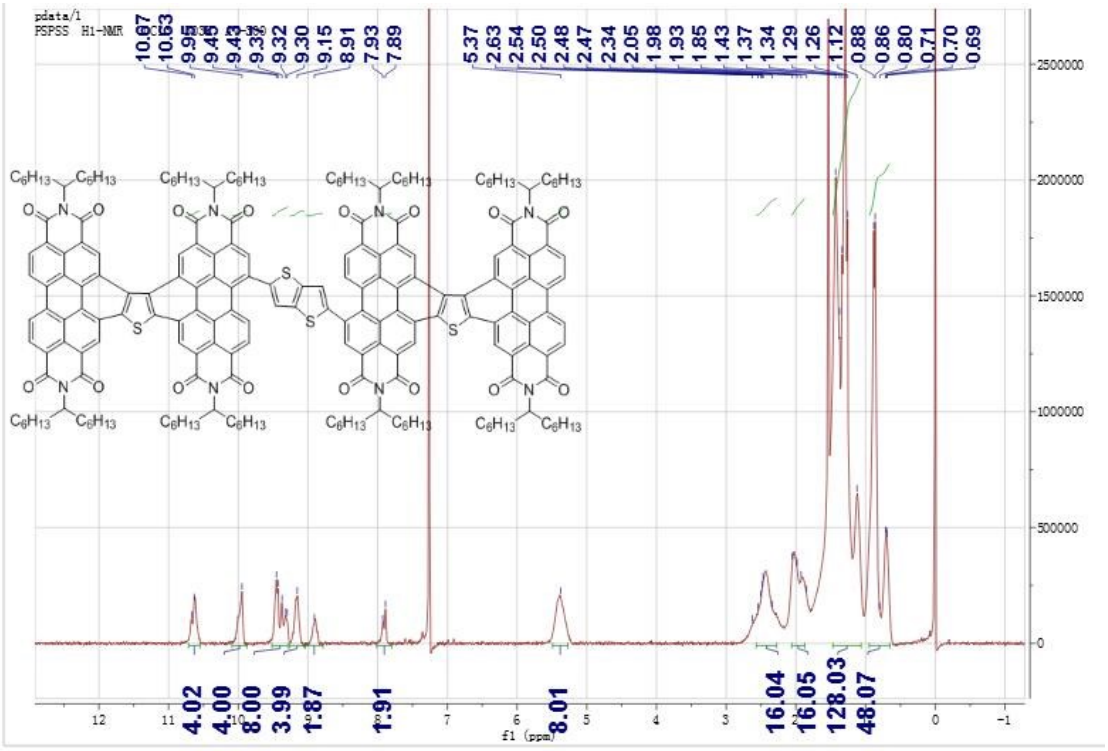

Figure S3. ^{1}H NMR spectrum of P_4TT2T.

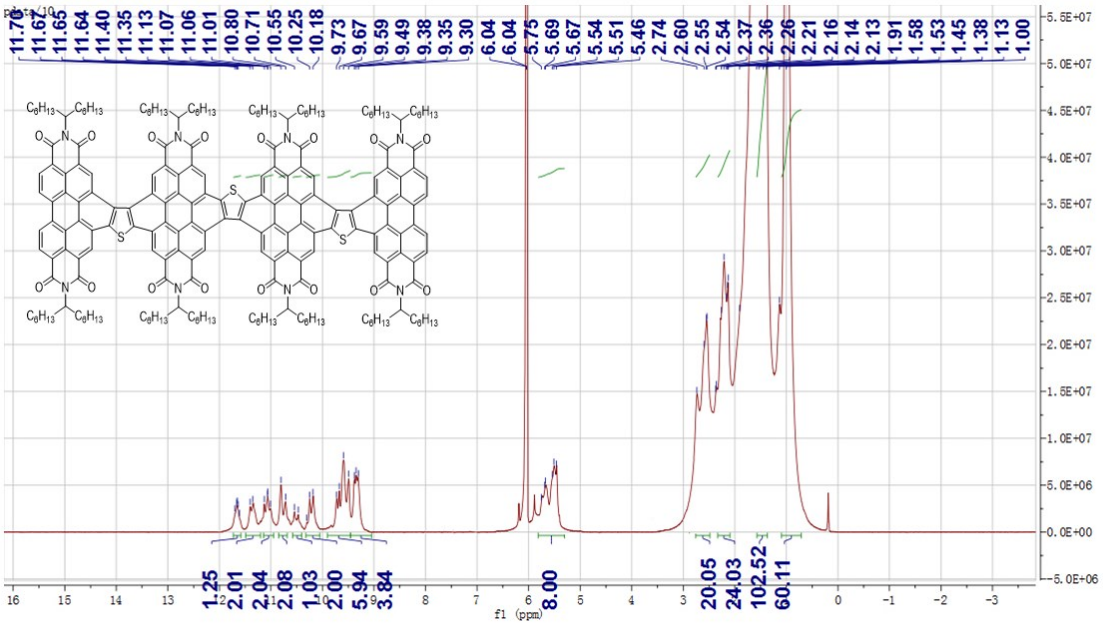

Figure S4. ^{1}H NMR spectrum of $FP_4 3T$.

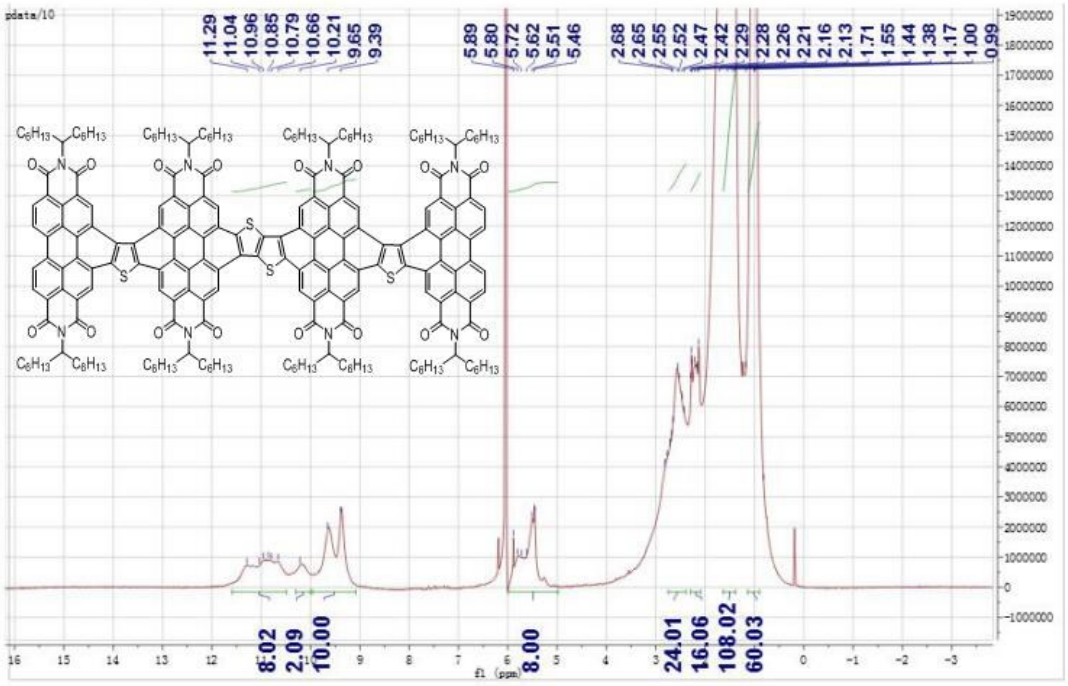

Figure S5. ^{1}H NMR spectrum of FP_4TT2T.

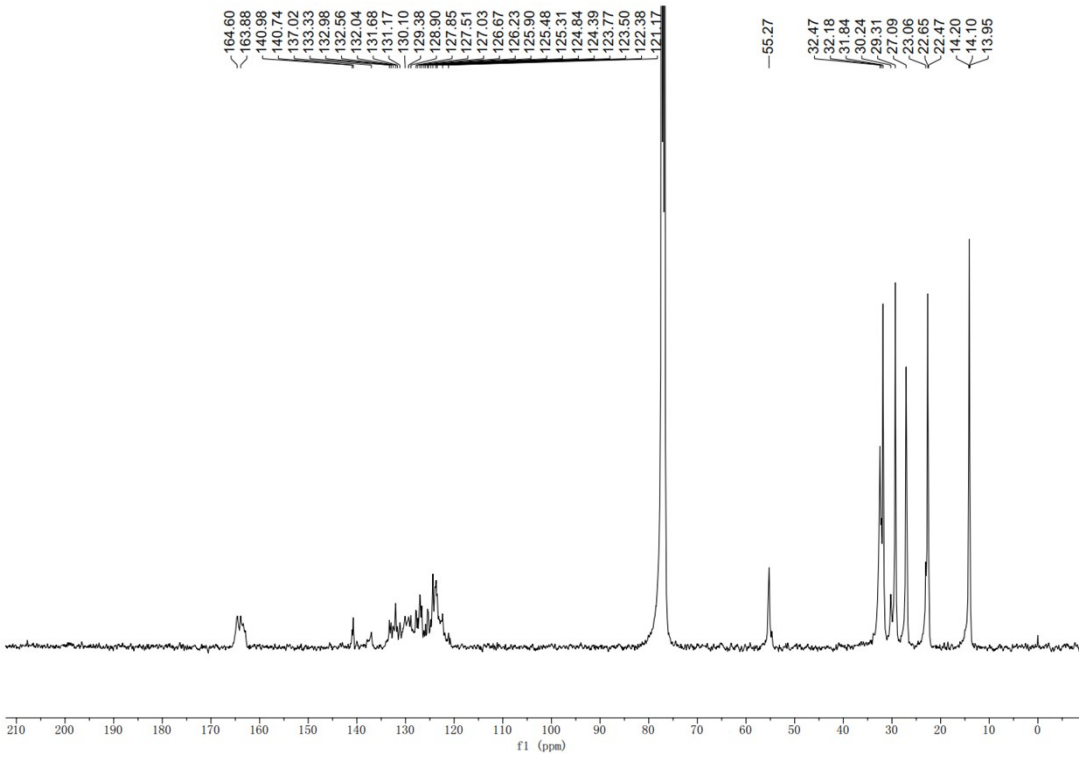

Figure S6. ^{13}C NMR of FPDI-T-Br.

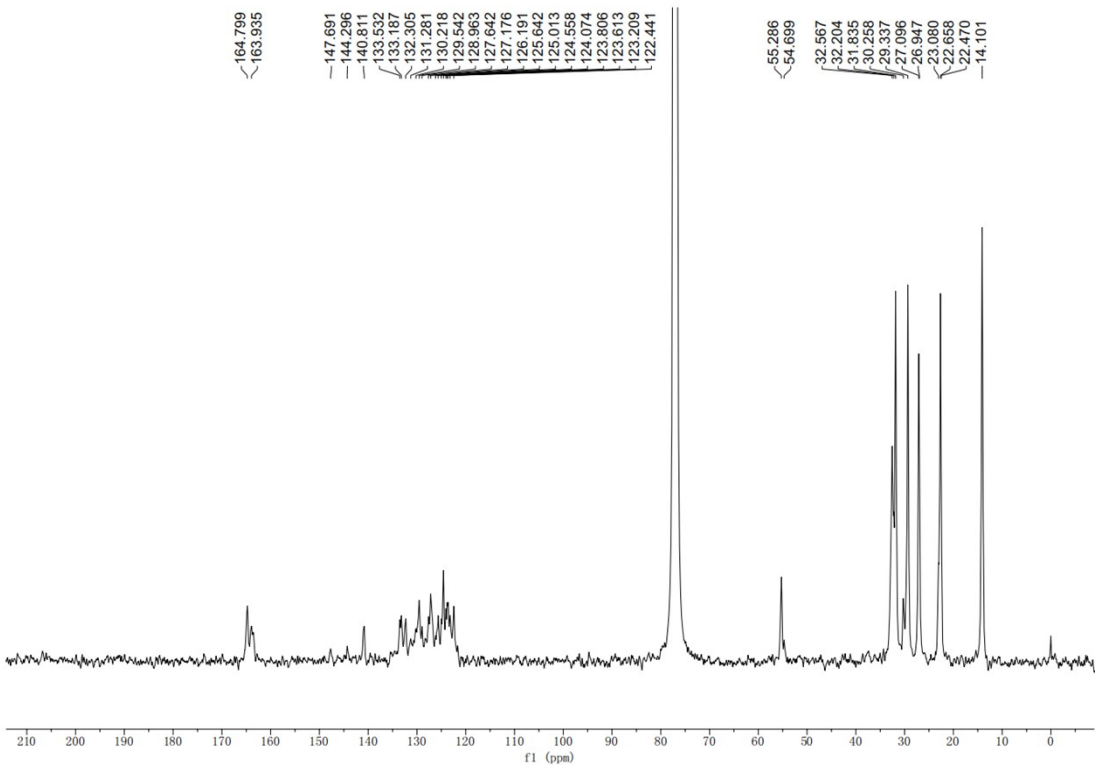

Figure S7. ^{13}C NMR of $P_4$3T.

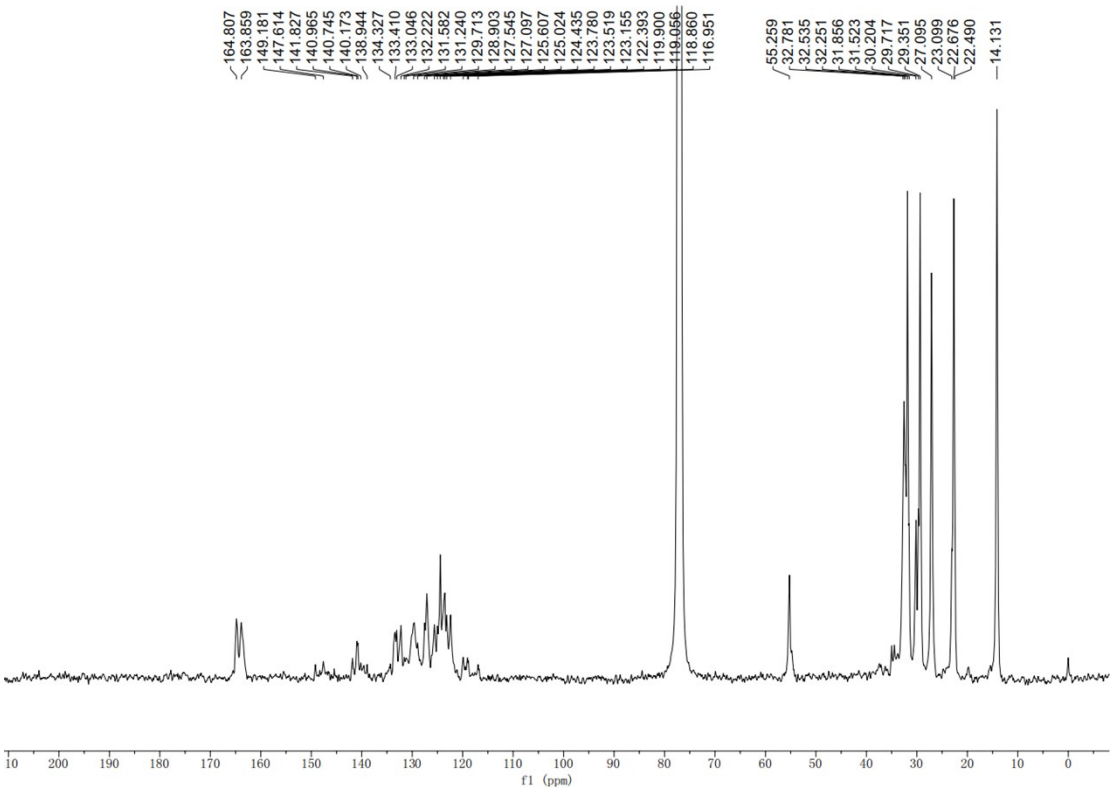

Figure S8. ^{13}C NMR of P_4TT2T.

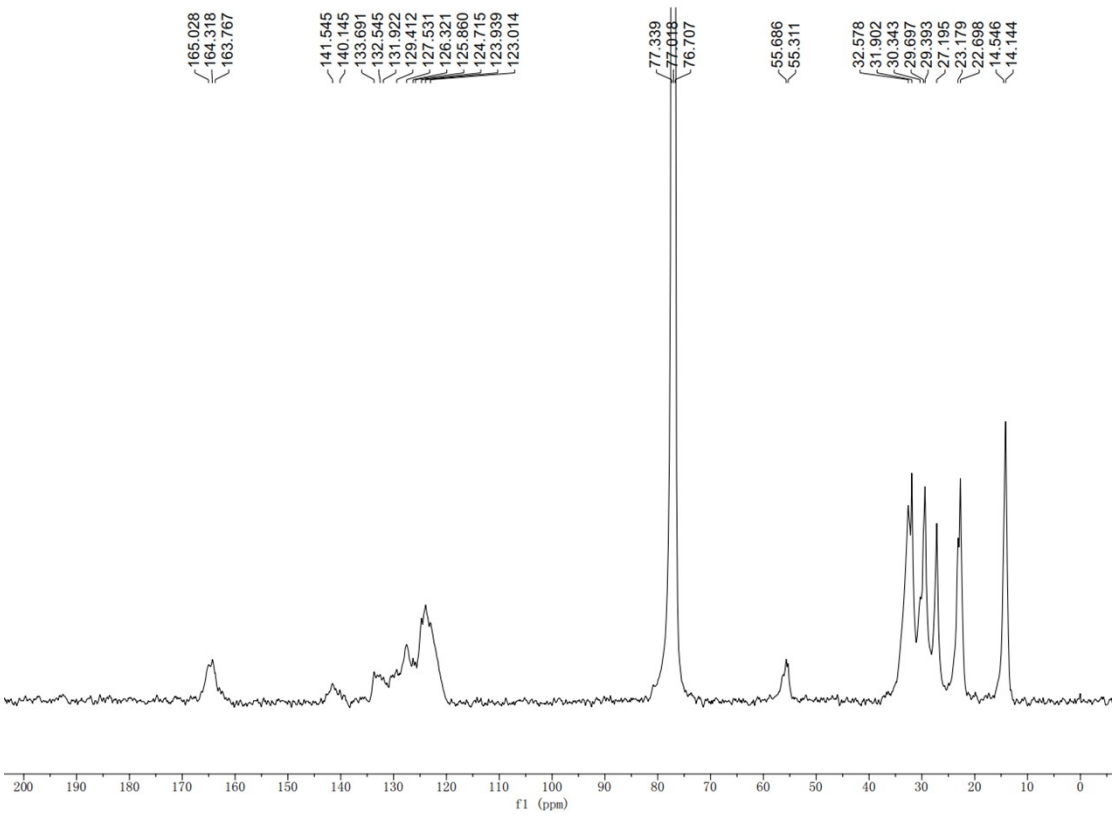

Figure S9. ^{13}C NMR of $FP_4$3T.

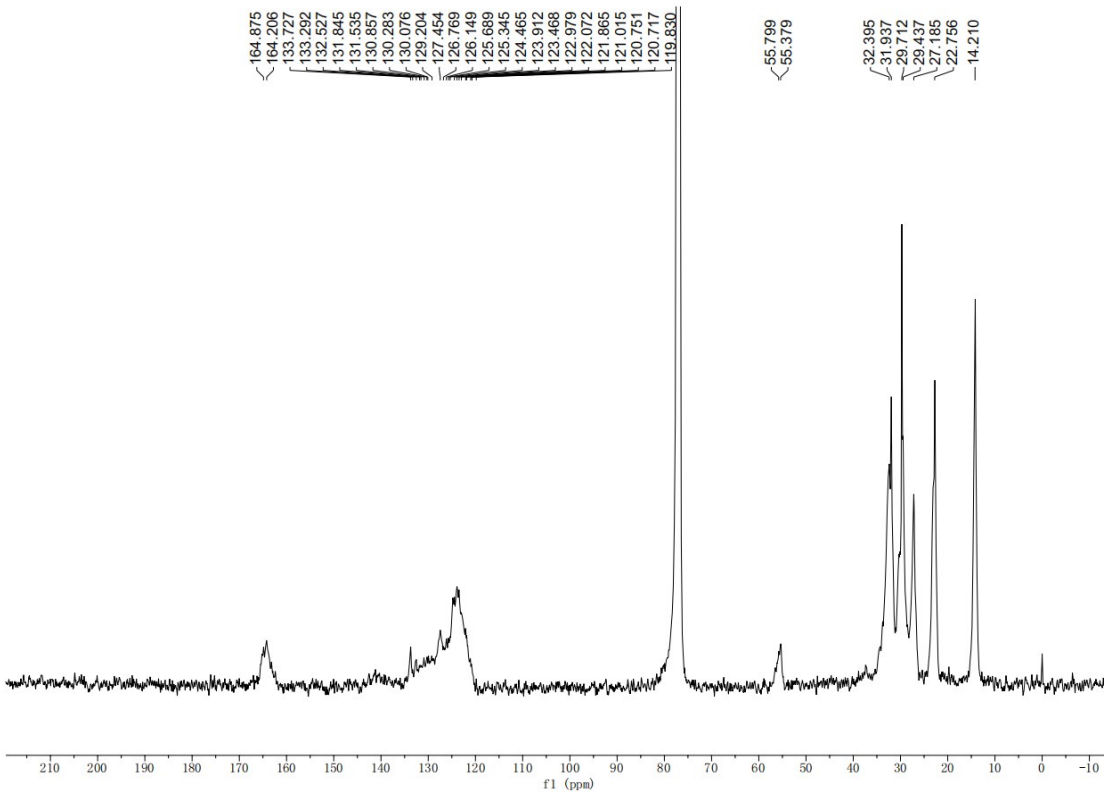

Figure S10. ^{13}C NMR of FP_4TT2T.

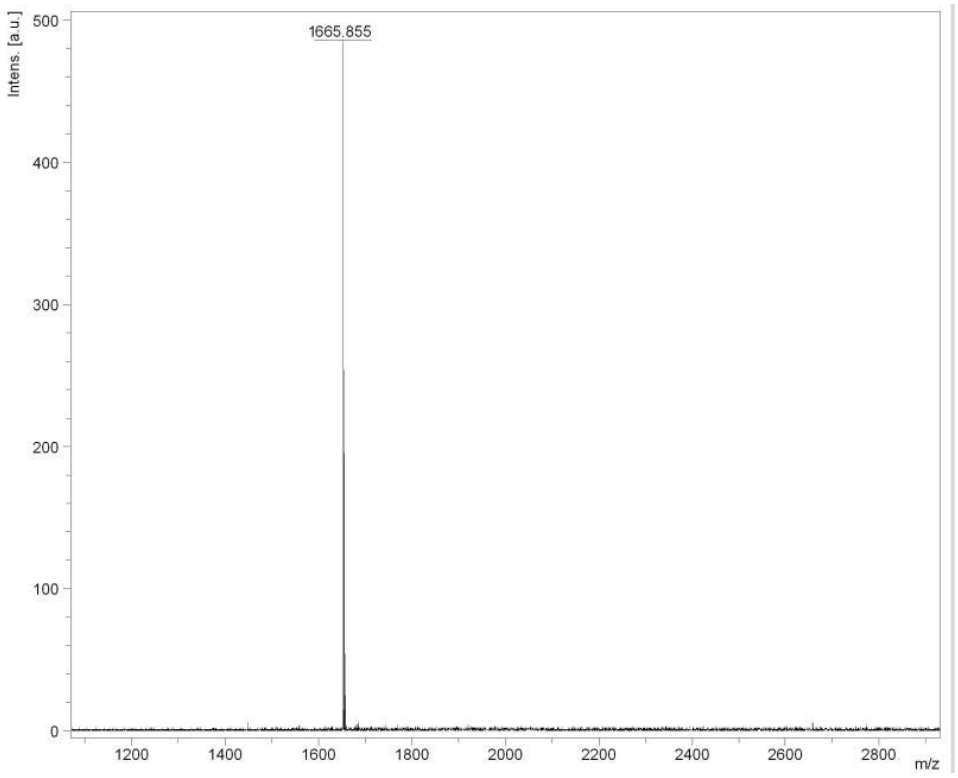

Figure S11. MALDI-TOF-MS of FPDI-T-Br.

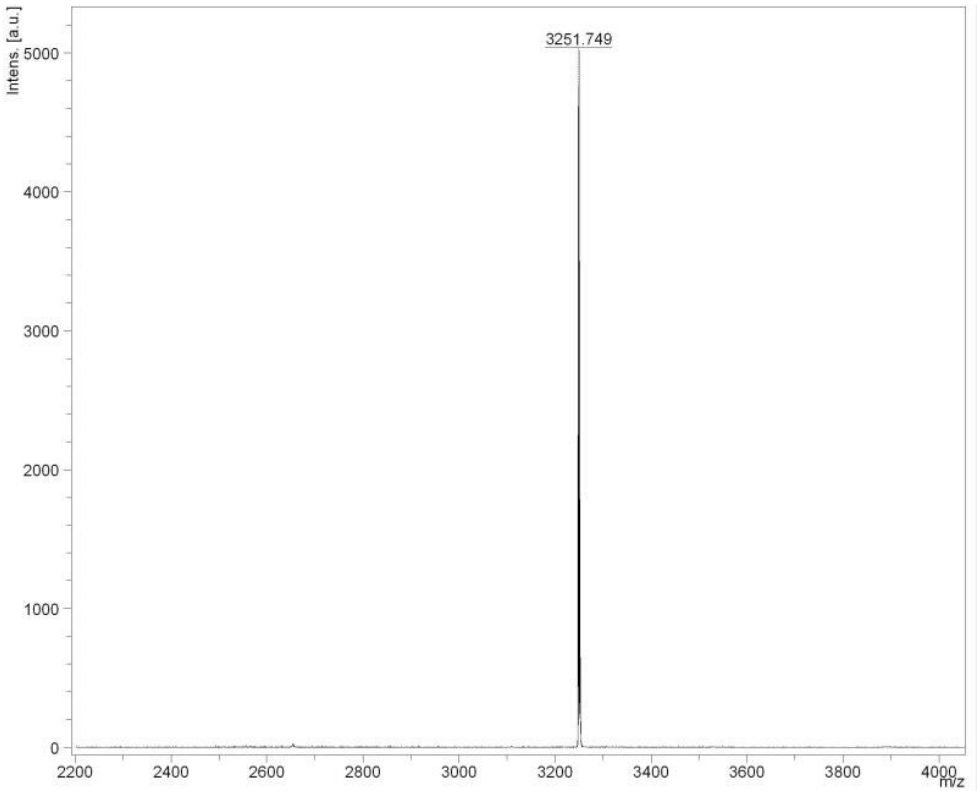

Figure S12. MALDI-TOF-MS of $P_4$3T.

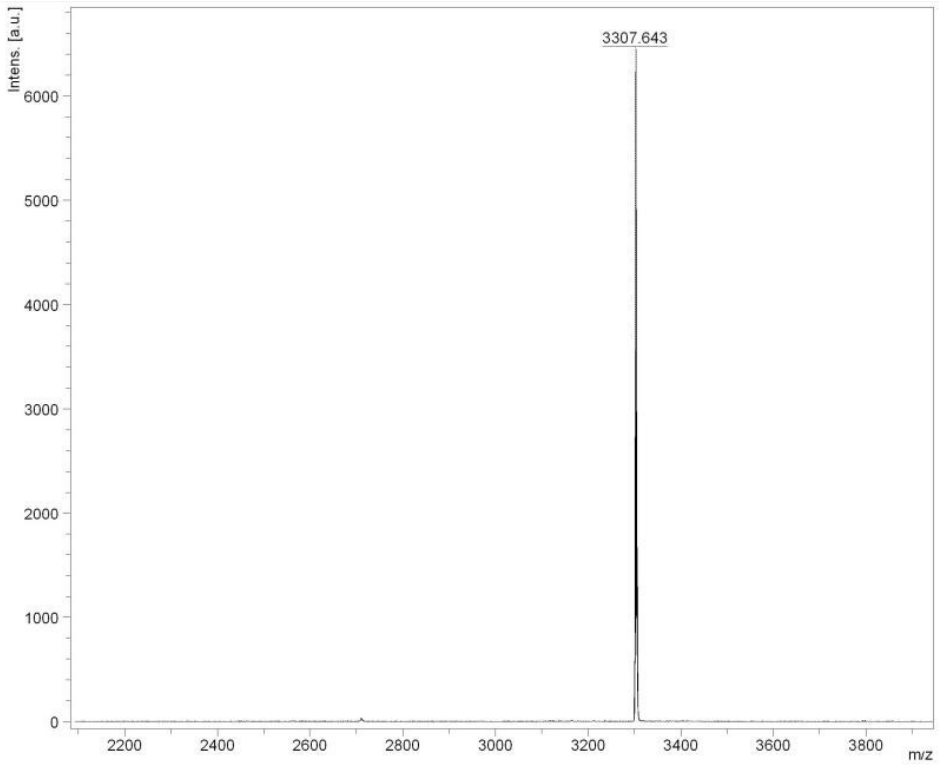

Figure S13. MALDI-TOF-MS of P_4TT2T.

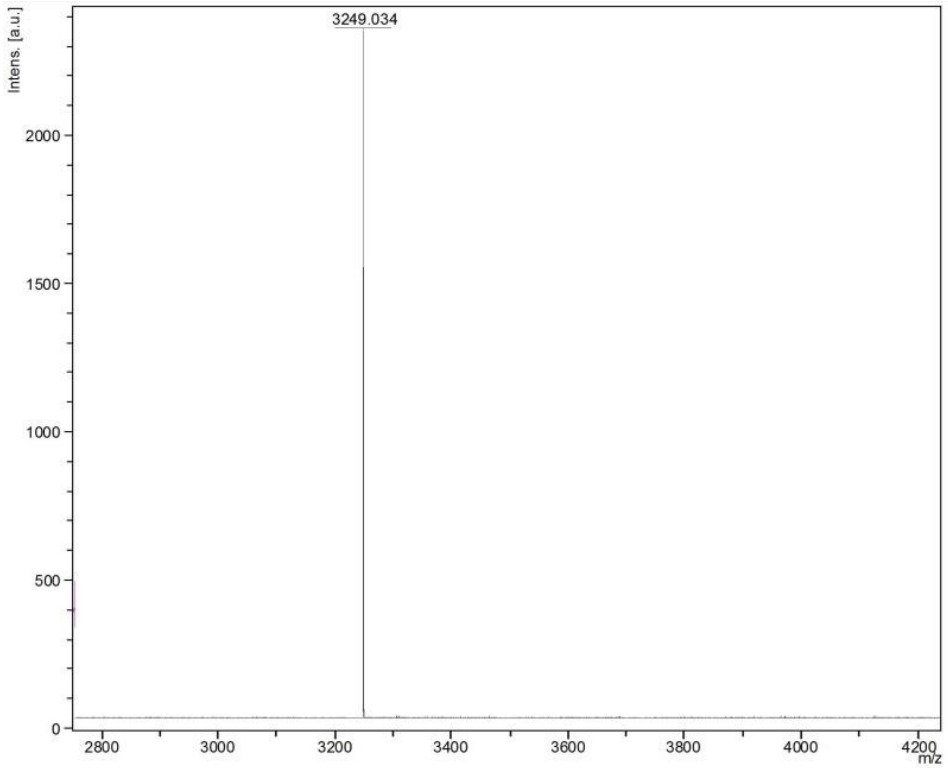

Figure S14. MALDI-TOF-MS of FP_43T.

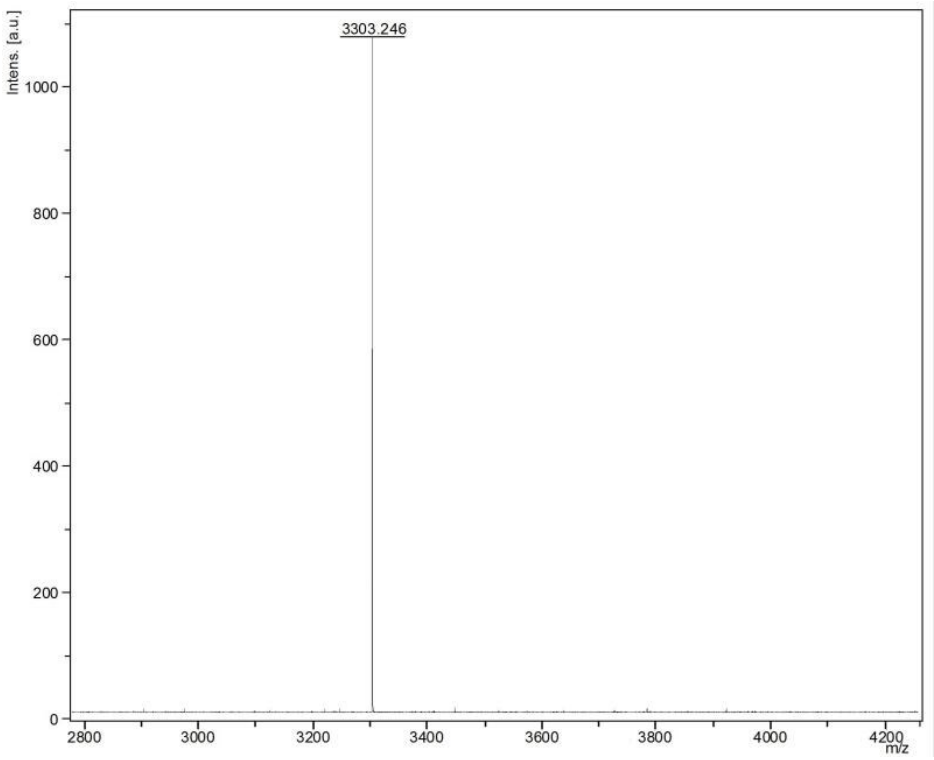

Figure S15. MALDI-TOF-MS of FP_4TT2T.

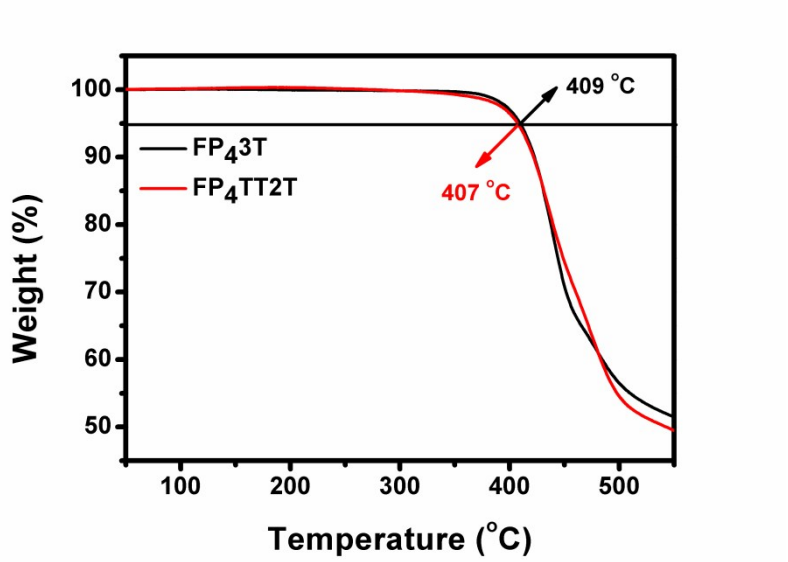

Figure S16. TGA curves of FP_43T and FP_4TT2T.

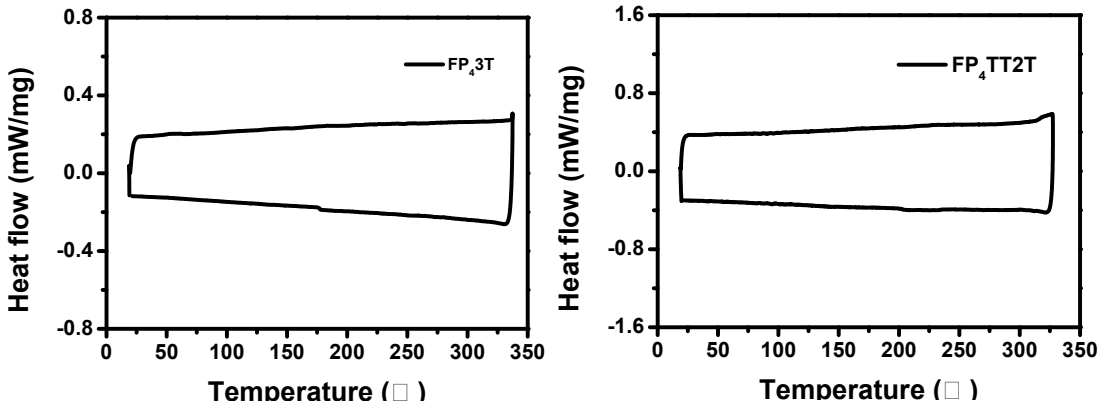

Figure S17. DSC curves of $FP_4$3T and FP_4TT2T.

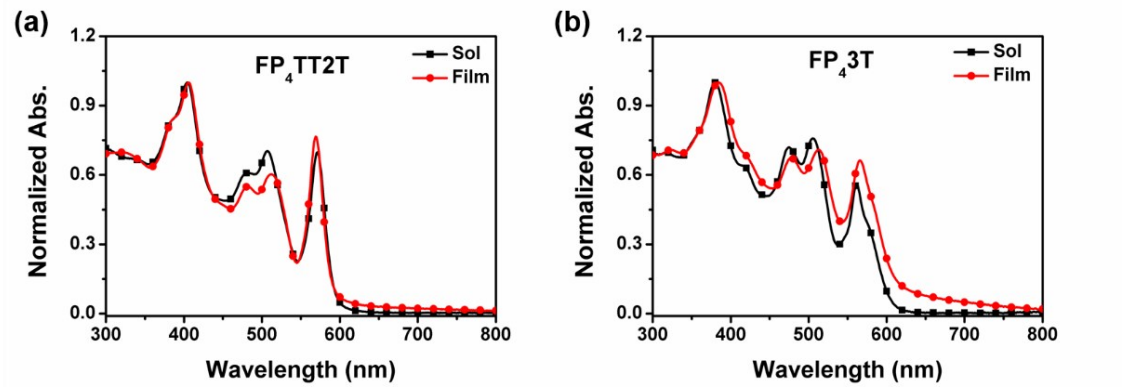

Figure S18. Absorption spectra of (a) FP_4TT2T and (b) $FP_4$3T in solution and film states.

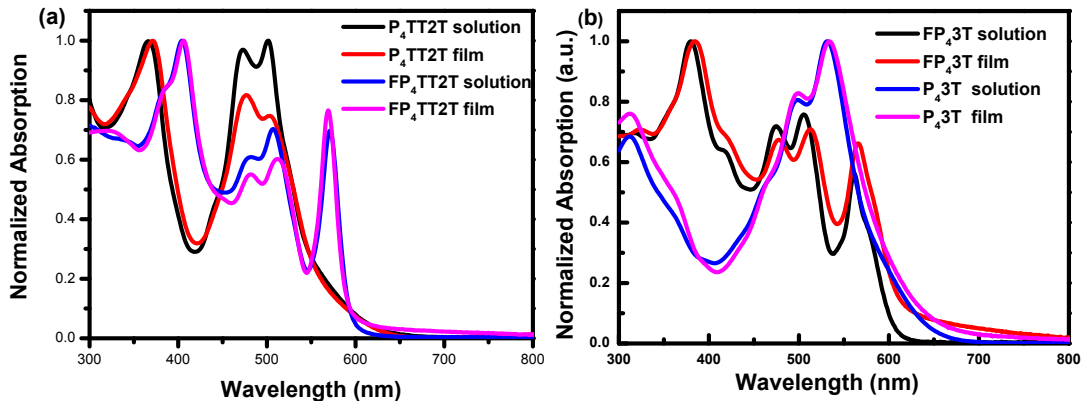

Figure S19. Absorption spectra of (a) P_4TT2T and FP_4TT2T (b) P_43T and FP_43T in solution and film states.

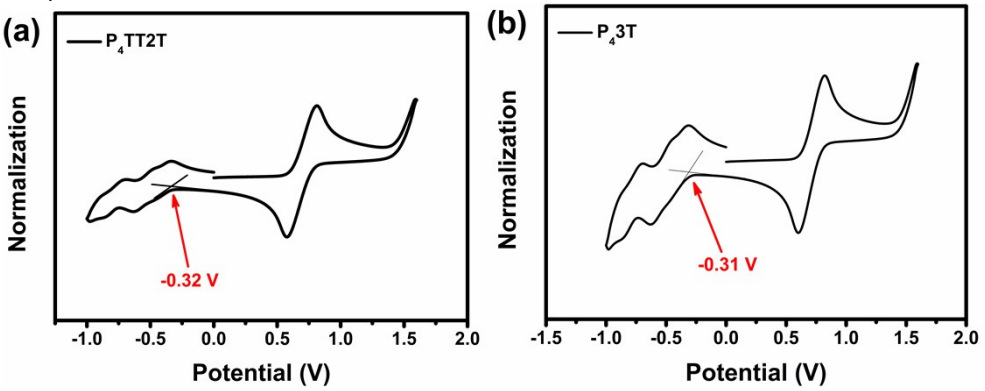

Figure S20. Cyclic voltammograms of P_4TT2T and P_43T measured in 0.1 M solutions of tetra-*n*-butylammonium hexafluorophosphate in dry dichloromethane.

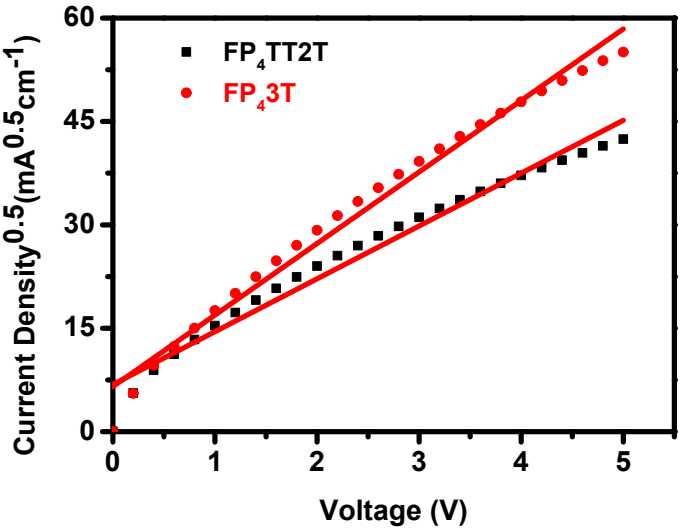

Figure S21. $J^{0.5}$-V curves of hole-only devices based on FP_43T:PTB7-Th and FP_4TT2T:PTB7-Th films.

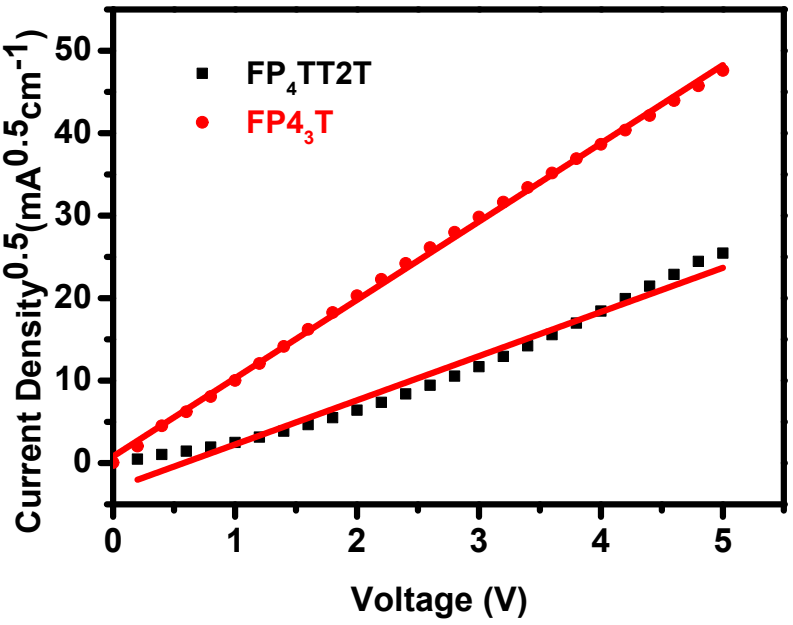

Figure S22. $J^{0.5}$-V curves of electron-only devices based on $FP_4$3T:PTB7-Th and FP_4TT2T:PTB7-Th films.

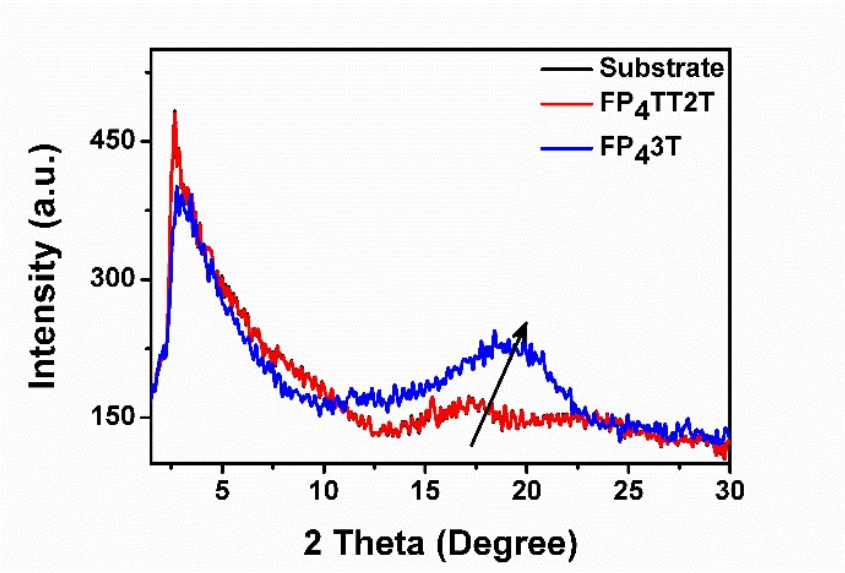

Figure S23. XRD patterns of FP_4TT2T and $FP_4$3T films.

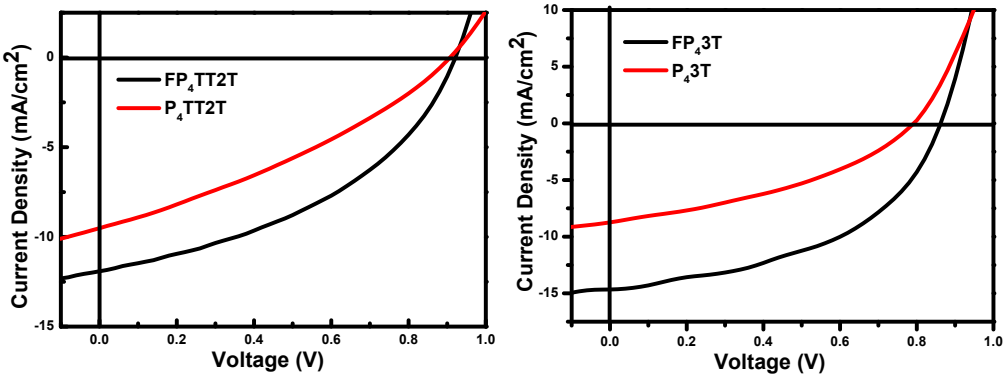

Figure S24. *J-V* curves of the PTB7-Th:P_4TT2T, PTB7-Th:FP_4TT2T, PTB7-Th:P_43T, PTB7-Th:FP_43T based optimal solar cells devices under AM 1.5G irradiation (100 mW cm^{-2}).

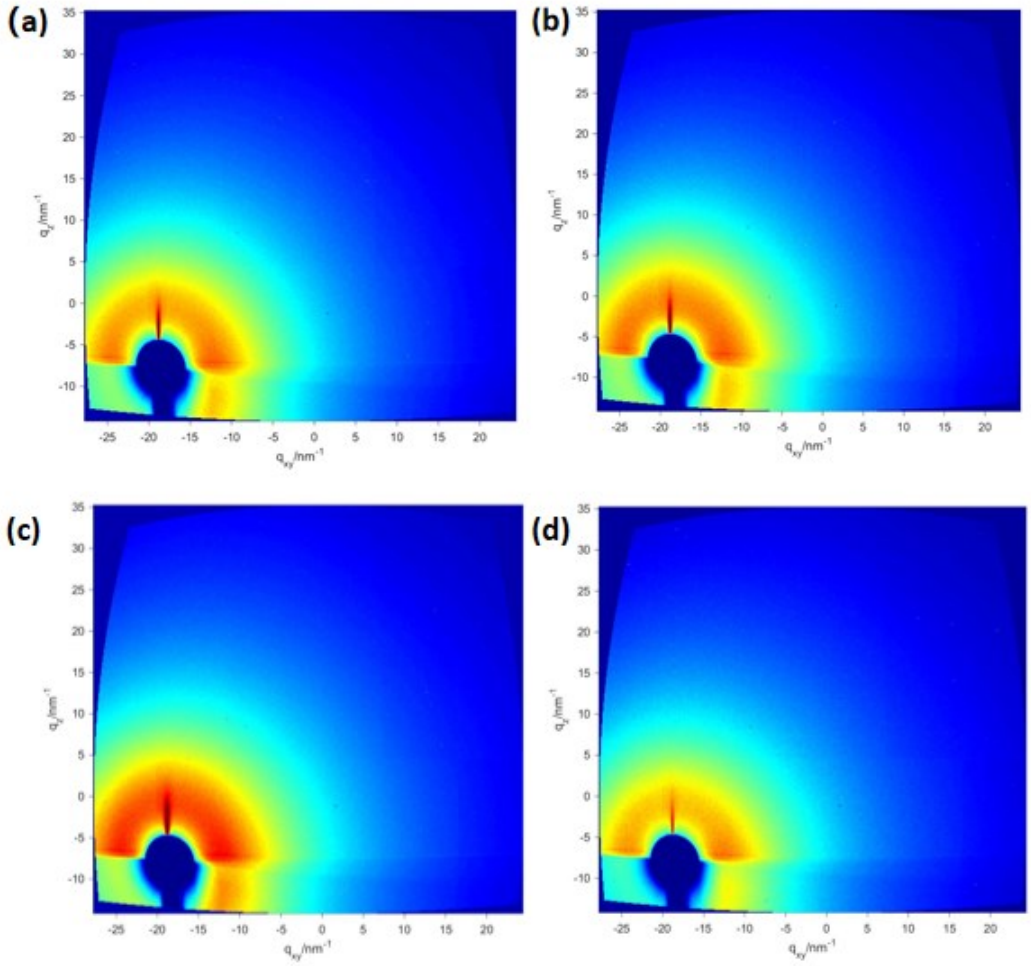

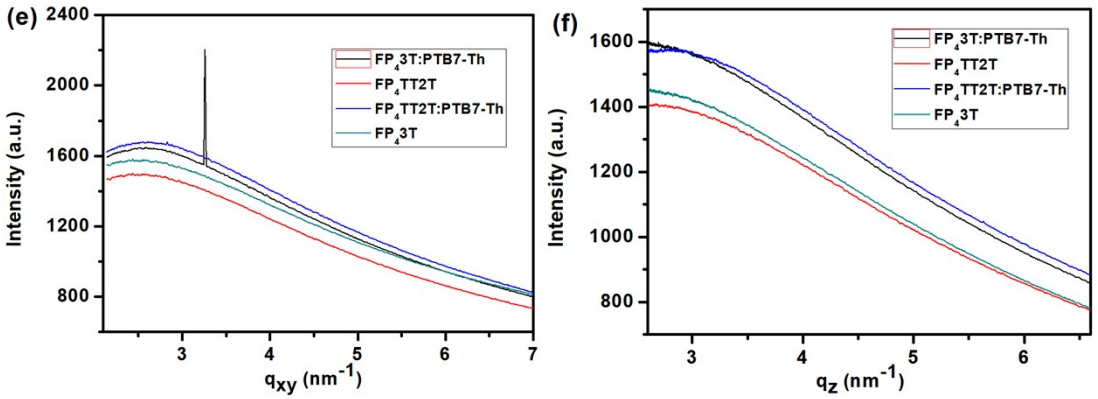

Figure S25. 2D GIXRD patterns of (a) the neat $FP_4$3T film (b) the PTB7-Th:$FP_4$3T (1:1, w/w) blend film (c) the neat FP_4TT2T film (d) the PTB7-Th:FP_4TT2T (1:1, w/w) blend films. (e) The in-plane and (f) out-of-plane cuts of the corresponding 2D GIXRD patterns.

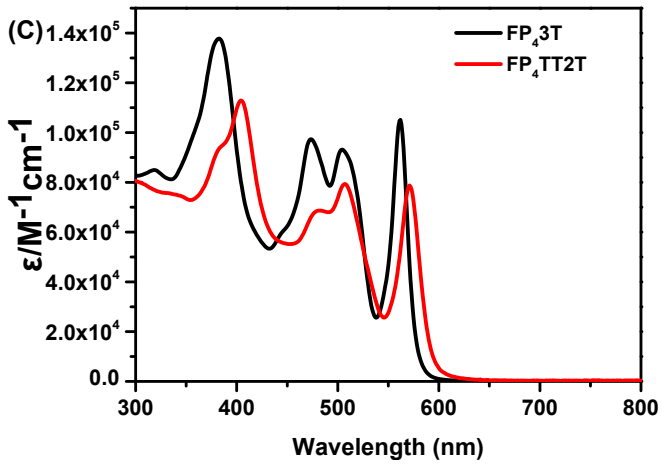

Figure S26. UV-visible absorption spectra of FP_4TT2T and $FP_4$3T in CH_2Cl_2 solution.

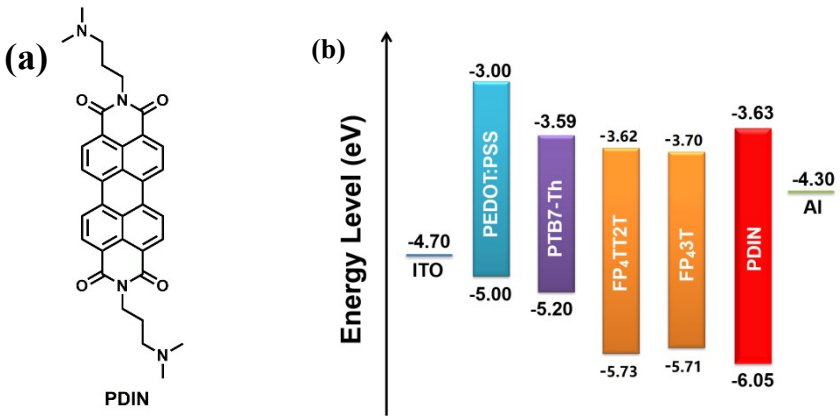

Figure S27. (a) Chemical structure of PDIN. (b) Energy levels of different layers in the BHJ-OSCs.

Table S1. Optical and electrochemical properties of P_4TT2T, FP_4TT2T, $P_4$3T and $FP_4$3T.

Material	*λmax (sol)* [nm] [a]	*λmax (film)* [nm]	*Ered onset* [V] [b]	LUMO [eV] [c]	Bandgap [eV] [d]	HOMO [eV] [e]
P4TT2T	366	371	-0.32	-3.76	2.12	-5.88
FP_4TT2T	404	406	-0.50	-3.62	2.11	-5.73
P43T	531	533	-0.31	-3.77	2.00	-5.77
$FP_4$3T	380	385	-0.42	-3.70	2.01	-5.71

[a] Obtained in CH_2Cl_2 solution; [b] Measured by cyclic voltammetry; [c] Calculated by using LUMO = −[*E*red onset − $E_{Fc/Fc+}$ + 4.8] eV; [d] Estimated based on film absorption onset; [e] Calculated by using LUMO and *E*g opt.

Table S2. Photovoltaic performances of PTB7-Th:P_4TT2T, PTB7-Th:FP_4TT2T, PTB7-Th:$P_4$3T and PTB7-Th:$FP_4$3T solar cells, under illumination of AM1.5G (100 mW cm^{-2}).

D:A [a]	V_{OC} [V]	J_{SC} [mA cm^{-2}]	FF [%]	PCE [%] [b]
PTB7-Th:P4TT2T	0.91	9.5	32.6	2.82(2.67)
PTB7-Th:FP_4TT2T	0.92	11.9	42.1	4.62 (4.34)
PTB7-Th:P43T	0.79	8.7	38.3	2.63 (2.38)
PTB7-Th:$FP_4$3T	0.86	14.7	48.1	6.05 5.92)

[a] The optimized donor-to-acceptor ratio was 1:1 (w/w%); [b] The average data obtained from analysis of 10 devices are shown in brackets.

Reference

1. H. Zhong, C.-H. Wu, C.-Z. Li, J. Carpenter, C.-C. Chueh, J.-Y. Chen, H. Ade and A. K.-Y. Jen, *Adv. Mater.*, **2016**, 28, 951-958.
2. M.J. Frisch, G. Trucks, H. Schlegel, G. Scuseria, M. Robb, J. Cheeseman, G. Scalmani, V. Barone, B. Mennucci, G.J.I.W. Petersson, CT, Gaussian 09, Revision D. 01, Gaussian, (2009).
3. M. Gg., B. Pj., C. Scott, S. Jr., *Phys. Rev. B*, **1998**, *581*, 10371.